Soft Matter

Accepted Manuscript

This is an *Accepted Manuscript*, which has been through the Royal Society of Chemistry peer review process and has been accepted for publication.

Accepted Manuscripts are published online shortly after acceptance, before technical editing, formatting and proof reading. Using this free service, authors can make their results available to the community, in citable form, before we publish the edited article. We will replace this *Accepted Manuscript* with the edited and formatted *Advance Article* as soon as it is available.

You can find more information about *Accepted Manuscripts* in the **Information for Authors**.

Graphical Abstract

1
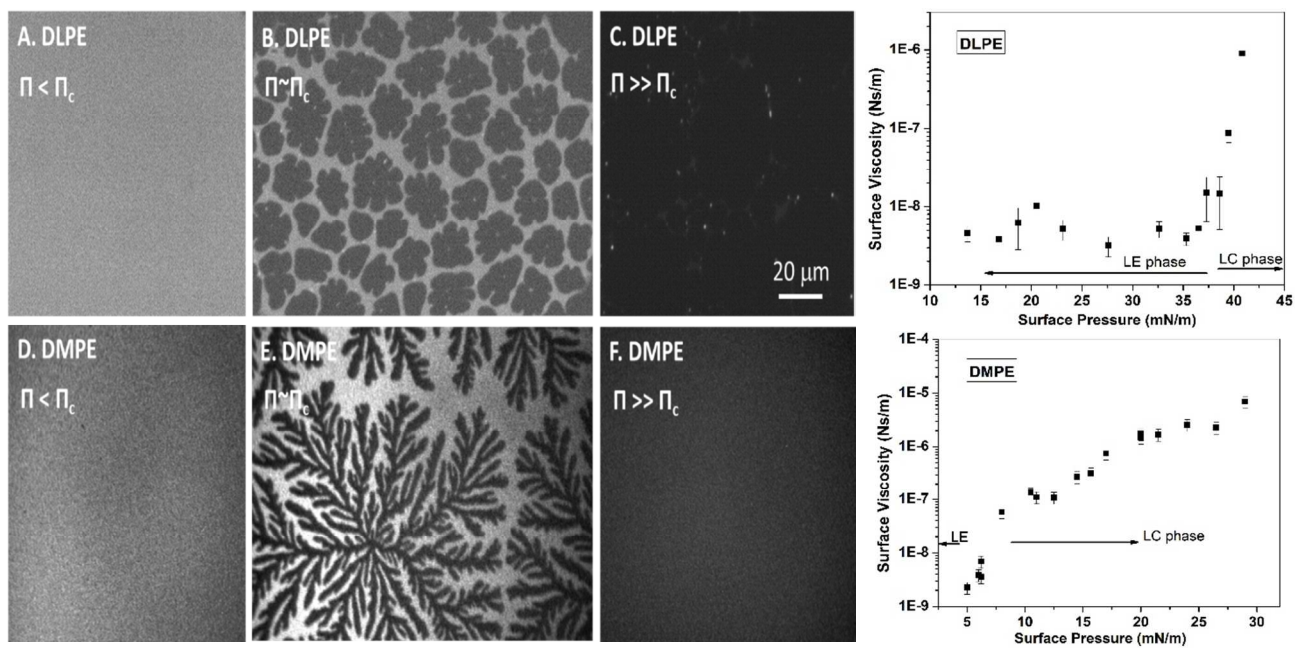
Monitoring Phases and Phase Transitions in Phosphatidylethanolamine Monolayers Using Active Interfacial Microrheology

Saba Ghazvini[1], Brandon Ricke[1], Joseph A. Zasadzinski[2] and Prajnaparamita Dhar[1]*

[1] Department of Chemical Engineering, University of Kansas, Lawrence KS 66045.

[2] Chemical Engineering and Materials Science, University of Minnesota, Minneapolis, Minnesota 55455.

*to whom correspondence should be addressed: Email: prajnadhar@ku.edu

Abstract:

Active interfacial microrheology is a sensitive tool to detect phase transitions and headgroup order in phospholipid monolayers. The re-orientation of a magnetic nickel nanorod is used to explore changes in the surface rheology of 1,2-dilauroyl-sn-glycero-3-phosphoethanolamine (DLPE) and 1,2-dimyristoyl-sn-glycero-3-phosphoethanolamine (DMPE), which differ by two CH_2 groups in their alkyl chains. Phosphatidylethanolamines such as DLPE and DMPE are a major component of cell membranes in bacteria and in the nervous system. At room temperature, DLPE has a liquid expanded (LE) phase for surface pressure, $\Pi < \sim 38$ mN/m; DMPE has an LE phase for $\Pi < \sim 7$ mN/m. In their respective LE phases, DLPE and DMPE show no measurable change in surface viscosity with Π, consistent with a surface viscosity $< 10^{-9}$ Ns/m, the resolution of our technique. However, there is a measurable, discontinuous change in the surface viscosity at the LE to liquid condensed (LC) transition for both DLPE and DMPE. This discontinuous change is correlated with a significant increase in the surface compressibility modulus (or isothermal two-dimensional bulk modulus). In the LC phase of DMPE there is an exponential increase in surface viscosity with Π consistent with a two-dimensional free area model. The second-order LC to solid (S) transition in DMPE is marked by an abrupt onset of surface elasticity; there is no measurable elasticity in the LC phase. A measureable surface elasticity in the S phase suggests a change in the molecular ordering or interactions of the DMPE headgroups that is not reflected in isotherms or in grazing incidence X-ray diffraction. This onset of measureable elasticity is also seen in DLPE, even though no indication of a LC-S transition is visible in the isotherms.

3

Introduction:

Phosphatidylethanolamines (PE) make up a substantial fraction of the lipids in the central nervous system, such as the white matter of brain, nerves, neural tissue, and in the spinal cord. In contrast to phosphatidylcholine, PE is concentrated with phosphatidylserine in the inner or cytoplasmic monolayer of the plasma membrane [1]. PE is also the dominant lipid in bacterial cell membranes; specific interactions with PE are often essential to development of new antimicrobial medications [2]. PE and other phospholipid monolayers exhibit a range of structural polymorphs [3] that can be readily accessed in a Langmuir trough by altering the area occupied by a fixed number of molecules at the air-water interface. Understanding the structure-property relationships of Langmuir films provides insight into the properties of PE in biomembranes as well as in a variety of liquid-vapor interfaces common to the chemical, petroleum, and food industries [4]. Often, the goal in these studies is to determine how the shape, size and chemical features of the molecules that make up the films influence the organization, range and perfection of molecular ordering, and how these change with surface pressure and temperature.

Modern grazing incidence synchrotron X-ray diffraction (GIXD) has become a preferred method to determine molecular packing in different phases as well as the extent of molecular order, and how these change at phase transitions [5, 6]. However, well before the development of synchrotron X-ray sources, Harkins and coworkers showed that monolayer rheology could identify phase transitions or molecular rearrangements that were not obvious from Langmuir isotherms [7]. Slight differences in the molecular lattice or molecular tilt are often accompanied by significant changes in the surface viscosity of fatty acid [8] and fatty alcohol [9, 10] films. Similar changes in surface rheology are expected at phase transitions in phospholipid monolayers [11]; in particular, second order phase transitions in phospholipid monolayers are difficult to detect from

4

Langmuir isotherms and involve only subtle changes in X-ray diffraction patterns [5]. However, the interfacial rheology of these biologically relevant films has not been systematically examined due to their much lower surface viscosity and elasticity.

The smaller the surface viscosity, the harder it is to decouple the response of the two-dimensional interfacial film from that of the three-dimensional subphase [12-17]. This decoupling is quantified by the Boussinesq number, B, which is the ratio of surface to bulk drag on a probe of characteristic dimension, a (here the length of the nanorod):

$$B = \frac{\eta_s}{(\eta_w + \eta_a)a} \approx \frac{\eta_s}{\eta_w a} \qquad (1)$$

η_s is the surface viscosity; η_w and η_a are the bulk viscosities of water and air ($\eta_w \gg \eta_a$). Reliable measurements of surface viscosity require $B \gg 1$. Detailed analysis by Reynaert et al. show that current surface rheometers with macroscopic probes [18-20] (such as those used by Harkin and others), can be used to measure $\eta_s > 10^{-6}$ N-s/m [21]. Since phospholipid films in the liquid-expanded (LE) phase have surface viscosities of 10^{-9} N-s/m or lower [14-17, 22-24], the LE phase is inaccessible to macroscopic interfacial rheometers. As a result, the flow behavior of a significant portion of the phospholipid monolayer phase space remains unexplored. Introduction of new passive and active microrheology techniques using micron and even nanometer size probes [25] have increased the sensitivity of interfacial rheometers [26-31] by two to three orders of magnitude compared to commercial rheometers with a sensitivity of 10^{-6} N-s/m [14-17], making the current work possible.

The reorientation of a nickel nanorod (diameter = 300nm, length ~ 3-50 μm) due to an externally applied magnetic field was used to measure surface viscosity and detect elasticity. The nanometer dimensions of the probe decreases a and increases B for a given value of η_s in Eqn. 1,

allowing reliable measurements of surface viscosity as low as 10^{-9} Ns/m. By extending the

Fischer model for analyzing the motion of an object at an interface with a finite immersion depth

[32] to the motion of infinitely thin cylinders at an interface, it is possible to relate the drag on a

nanorods to the Boussinesq number, and hence, the surface viscosity[29]. Increasing the applied

external torque allows measurements of η_s of 10^{-5} Ns/m or higher. Here we present the surface

viscosity of two phosphatidylethanolamine monolayers, DLPE and DMPE, over a range of

surface pressures that include the liquid expanded (LE) phase, liquid condensed (LC) phase and

the LC-solid (S) phase transition, using a recently developed magnetic nanorod microrheometer

[26]. DLPE and DMPE have identical headgroups and differ by two CH2 groups per alkyl chain,

which leads to significant difference in the surface pressure at which phase transitions occur.

Detailed structural characterization by grazing incidence X-ray diffraction and surface pressure-

area isotherms and morphological information of both DLPE and DMPE are available [5, 33],

allowing us to correlate our surface viscosity measurements with molecular structure.

We find that the surface viscosity of both DLPE and DMPE undergo several orders of

magnitude change in surface shear viscosity with surface pressure in the LC and S phases. The

measured surface viscosity does not change with surface pressure in the LE phase, suggesting

that it is below our sensitivity limit of $\sim 10^{-9}$ N-s/m. However, the first order LE-LC phase

transition is accompanied by a measurable, discontinuous jump in the surface viscosity, and the

surface viscosity increases exponentially with surface pressure in the LC phase. The second

order transition from LC to S phase in both DMPE and DLPE is accompanied by an abrupt

appearance of elasticity in the film. The second order LC-S phase transition in PE films is easy to

miss in isotherms, but synchrotron X-ray diffraction shows that the molecular tilt disappears at

the LC-S transition for DMPE [5, 34] (see Supplemental Materials). However the dramatic onset of

elasticity makes the transition macroscopically obvious. It is not clear if the untilting (and the transition to hexagonal from orthorhombic symmetry) is sufficient to create a jump in monolayer elasticity or if the untilting is accompanied by a change in headgroup ordering due to enhanced hydrogen bonding between PE headgroups, which cannot be detected by X-ray diffraction.

Materials and Methods

Materials:

HPLC grade chloroform solutions of 1,2-dilauroyl-sn-glycero-3-phosphoethanolamine (DLPE) and 1,2-dimyristoyl-sn-glycero-3-phosphoethanolamine (DMPE) were purchased from Avanti Polar Lipids, Alabaster, AL, and used as received. Texas Red® 1,2-dihexadecanoyl-*sn*-glycero-3-phosphoethanolamine, triethylammonium salt, (TXR-DHPE) was purchased in the dried form from Life Technologies (Invitrogen) and dissolved in HPLC grade chloroform. All organic solvents were purchased from Fisher Scientific. The subphase water (resistivity 18.2 MΩ/cm) was prepared using a Millipore Gradient System (Billerica, MA). The lipids were stored at -20 $^{\circ}$C when not in use.

Surface tension and surface compressibility modulus: A filter-paper Wilhelmy plate on a Langmuir trough (KSV-NIMA, Biolin Scientific) was used to measure the surface pressure as a function of area occupied by the phospholipid molecules. The 2-D isothermal bulk modulus, *β,* is the inverse of the isothermal compressibility modulus κ :

$$\beta = -A\left(\frac{\partial \Pi}{\partial A}\right)_T = A\left(\frac{\partial \gamma}{\partial A}\right)_T = \frac{1}{\kappa}$$

For a monolayer, the surface compressibility modulus is a measure of the ability of the monolayer to store mechanical energy as stress. Both β and κ are related to the second derivative of the free energy, G, ($\gamma = \left(\dfrac{\partial G}{\partial A}\right)_T$, $\beta = A\left(\dfrac{\partial^2 G}{\partial A^2}\right)_T$), which means that $\beta \to 0$ (or $\kappa \to \infty$) at the first order LE-LC transition. At a second order LC-S phase transition, the area/molecule, A, is continuous, but β changes discontinuously. The compressibility modulus was calculated from the isotherm data by taking numerical derivatives of the surface pressure vs. molecular area isotherms using the Differentiate tool in the Origin 8.6 graphical plotting software. The numerical derivatives were smoothed with a Fourier filter using 5 points.

Active Microrheology: The nickel nanorods used as probes were synthesized by electrochemical deposition of nickel into alumina templates [35], then magnetized, thoroughly cleaned, and dispersed in a 90% isopropyl alcohol, 10% water solution [26]. A 1 mg/ml solution of DLPE or DMPE with 1 wt% of TXR-DHPE in chloroform was used as a spreading solution. To initiate each experiment, 20-40 μl of the rod solution was deposited dropwise at the air/water interface in a Langmuir trough using a micropipette. The isopropyl alcohol was allowed to evaporate for 45 minutes; a population of nanorods was retained at the interface by capillary forces. Typically, this technique of spreading nanorods allows uniform spreading of the rods, and results in a very dilute distribution of about 1-2 nanorods in the field of view (150X150 μm). The fluorescence images discussed below also indicate that this dilute concentration of rods at the surface does not disrupt the phospholipid domains. Next, the DLPE or DMPE /TXR-DHPE spreading solutions were added drop-wise from a micro-syringe onto the air/water interface, and the chloroform allowed to evaporate for 20 minutes. The films were compressed to the desired surface pressure using the barriers of the Lanmguir trough. Two sets of home-built electromagnetic coils, oriented

perpendicular to each other, capable of generating a magnetic field of 10-120G, were used to apply an external magnetic field to orient the nanorods. Individual rods were visualized with a Nikon E3800 microscope using a 50x long working distance objective. Videos of the rod reorientations were recorded with a CCD camera connected to a personal computer and digitized for analysis [26]. At each surface pressure two different directions of rod orientation, as well as multiple rod motions were analyzed. Each rod orientation involved analysis of up to 45 frames per second of video for dilute systems in the LE phase.

Analysis of nanorod motion: The orientation of a magnetic nanorod (length l, magnetic moment $\mu_o m$) due to an externally applied magnetic field, **H,** can be described by the angle, $\varphi(t)$, between the long axis of the rod and the direction of the applied field (the applied field direction is defined to be $\varphi = 0$). Typically, the magnetic field is first turned on through one set of coils, which describes the initial orientation of the rods, and then a perpendicular magnetic field is applied. This ensures that the result of drift at the interface does not interfere with the rod angular motion analysis. In a purely viscous medium, the magnetic field provides the torque needed to align the rod, which is resisted by the viscous drag on the rod [26]:

$$\mu_0 mH \sin\varphi = -f_r \eta_w l^3 \frac{d\varphi}{dt} \qquad (2)$$

the solution to which is:

$$\tan\left(\frac{\varphi}{2}\right) = \exp\left(\frac{-t}{\tau}\right) \qquad (3)$$

The relaxation time, $\tau = \frac{f_r \eta_w l^3}{\mu_0 mH}$, gives the dimensionless drag coefficient of the rod, $f_r = f_w + f_s$, which is a sum of the bulk water (f_w) and surface (f_s) drag. The magnetic moment of the

9

rod can be written in terms of the magnetization, *M,* and the rod aspect ratio, *l/r*, which gives the relaxation time, τ, as:

$$\tau = \frac{f_r \eta_w l^3}{\mu_0 mH} = \frac{f_r \eta_w l^3}{\mu_0 MVH} = \frac{f_r \eta_w l^3}{\mu_0 M \pi r^2 lH} = \frac{f_r \eta_w}{\mu_0 M \pi H}\left(\frac{l}{r}\right)^2 \qquad (4)$$

The magnetization of rods was calibrated by averaging the motion of several nanorods in water and glycerol solutions [29, 36, 37] and the average value of magnetization, $1.2 * 10^5$ ($\pm$ 0.5) A/m, was used for all subsequent experiments. The relaxation time τ, was obtained by fitting equation 3 to the measured values of rod orientation obtained by analyzing digitized videos of the rod motion using a particle tracking program and Origin 8.6. The subphase drag due to water, f_w, is taken to be equal to half that of the drag on a rod of radius *r* and length *l* (for $l/r \geq 20$) rotating in a viscous fluid [29, 36, 37]:

$$f_w = \frac{\pi}{6\left[\ln\left(\frac{l}{r} - 0.8\right)\right]}. \qquad (5)$$

Typically, $f_s \gg f_w$ in these experiments, suggesting that the measurements are sensitive to the interfacial stresses. The rod axial ratio, *l/r*, is the only relevant parameter needed to calculate f_w. For each value of τ, f_s was calculated by subtracting f_w from f_r. The relationship between the Boussinesq number, *B,* for a given f_s for an incompressible interfacial film was determined in Dhar et al. [29] and used to calculate the surface viscosity using Eqn. 1. The range of B values ranged from 0.1 in the LE phase to > 1000 at the end of the LC phase.

Elasticity, E_s, in the film adds a term proportional to $E_s\varphi$ to the right hand side of Eqn. 2, such that the torque balance equation now becomes:

10

$$\mu_0 mH \sin\varphi = -f_r \eta_w l^3 \frac{d\varphi}{dt} + E_s \left(\frac{\pi}{2} - \varphi\right) \tag{6}$$
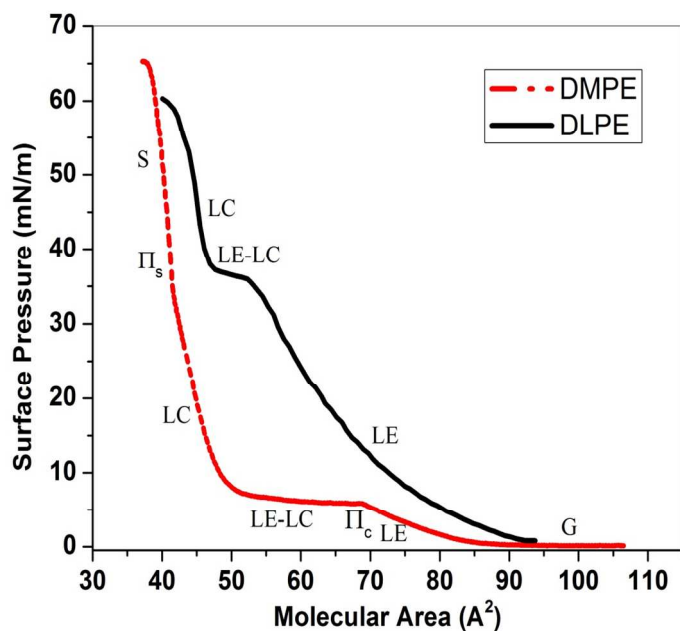

Figure 1a. Surface pressure vs. molecular area isotherm of DLPE(straight black line) and DMPE (dash red line) show the progression from a "gaseous" phase (G) at high areas per molecule to a liquid-expanded (LE) phase as the film is compressed (i.e. molecular area decreased) as reflected in the lift-off of the isotherm from Π=0. The LC phase is nucleated at $\Pi_c \sim$ 37 mN/m for DLPE and $\Pi_c \sim$ 7 mN/m for DMPE; further compression causes the LC phase to grow at the expense of the LE phase at roughly constant surface pressure. This coexistence plateau in the isotherm marks the first-order LE-LC transition. At the end of the plateau, compression rapidly increases the surface pressure in the LC phase and is related to a decrease in the molecular tilt and an increase in the crystalline order in the film. The second-order LC-solid (S) transition of DMPE corresponds to a kink in the isotherm and an increased slope at $\Pi_s \sim$ 34 mN/m.

A finite elasticity causes the rod to "stall" ($\frac{d\varphi}{dt} \to 0$) at a non-zero angle where the elastic force

is balanced by the magnetic torque (note that the magnetic torque goes to zero as $\varphi \to 0$ in Eqns.

3 and 5) [27, 38, 39]. To detect elasticity, as well as any anisotropic contribution from the monolayer

microstructure, torques were applied in both the x and y direction. For purely viscous

monolayers, the reorientation curves superimposed, the rod comes to rest aligned with the

applied magnetic field ($\varphi \to 0$), and the measured reorientation rate is well described by Eqn. 3

(Fig. 5). However, for viscoelastic monolayers, the reorientation in different directions did not

overlap, suggesting anisotropic ordering in the monolayer. The rod never aligned with the

applied field ($\varphi > 0°$ for $t \to \infty$ in Fig. 5), and Eqn. 3 did not fit the relaxation rate data.

Results and Discussion:

Figure 1a shows a representative surface pressure, $\Pi=\gamma_o-\gamma$, ($\gamma_o=72$ mN/m for water, γ is the measured surface tension) vs. molecular area isotherm of a DLPE (black curve) and DMPE (red curve) monolayers. As the area available to the monolayer is reduced, Π increases from zero, and the monolayer enters the disordered, liquid-expanded (LE) phase [40]. For the DLPE monolayer, continued compression causes the surface pressure to increase smoothly leading to a plateau at $\Pi_c \sim 37$ mN/m. DMPE (with two more methyl groups per chain than DLPE) plateaus
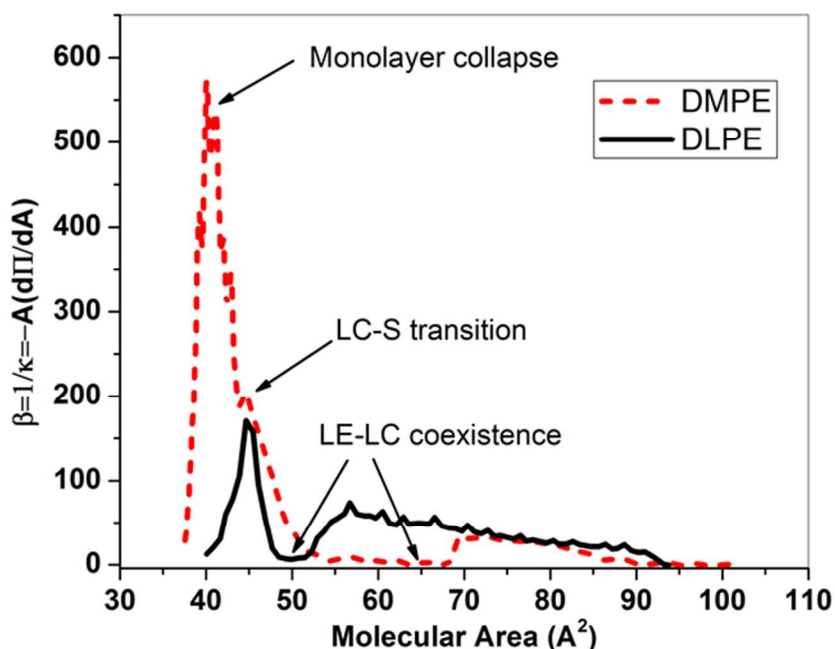

Figure 1b. Smoothened surface compressibility modulus vs. molecular area isotherm of DLPE (straight black line) and DMPE (dash red line) shows increasing compressibility modulus at the onset of the LE phase, and a sudden dip in the curve at values corresponding to the LE-LC coexistence plateau. A small discontinuity in the compressibility of DMPE corresponds to the kink in the surface pressure vs. area isotherm. The peak in the curves correspond to the onset of monolayer collapse, this is the close packed limit for the stable monolayer.

at $\Pi_c \sim 7$ mN/m. At Π_c, decreases in the area/molecule occur at a *nearly* constant surface pressure, which defines the LE-LC coexistence [3, 41]. Compression beyond the LE-LC coexistence plateau to surface pressures greater than Π_c results in an almost linear increase in the isotherm in the LC phase. In the LE phase at surface pressures below Π_c, there is steady increase in the bulk modulus, β, with decreasing area/molecule (Fig. 1b). However, at the LE-LC coexistence, β

goes to zero, consistent with a first order phase transition. β also undergoes a rapid linear increase with decreasing area/molecule and is significantly larger in the LC phase than the LE phase. GIXD of DMPE shows that these changes correlate with a decrease in the molecular tilt [4, 5]. The correlation length, which is a measure of the extent of the crystalline domains, also increases monotonically with increasing surface pressure [5]. A kink in the slope of the isotherm at Π_s, which is visible in DMPE isotherms but not DLPE, marks the second-order transition to the solid (S) phase in DMPE. Similarly, a small step in β at the same as Π_s is shown in Figure 1b.
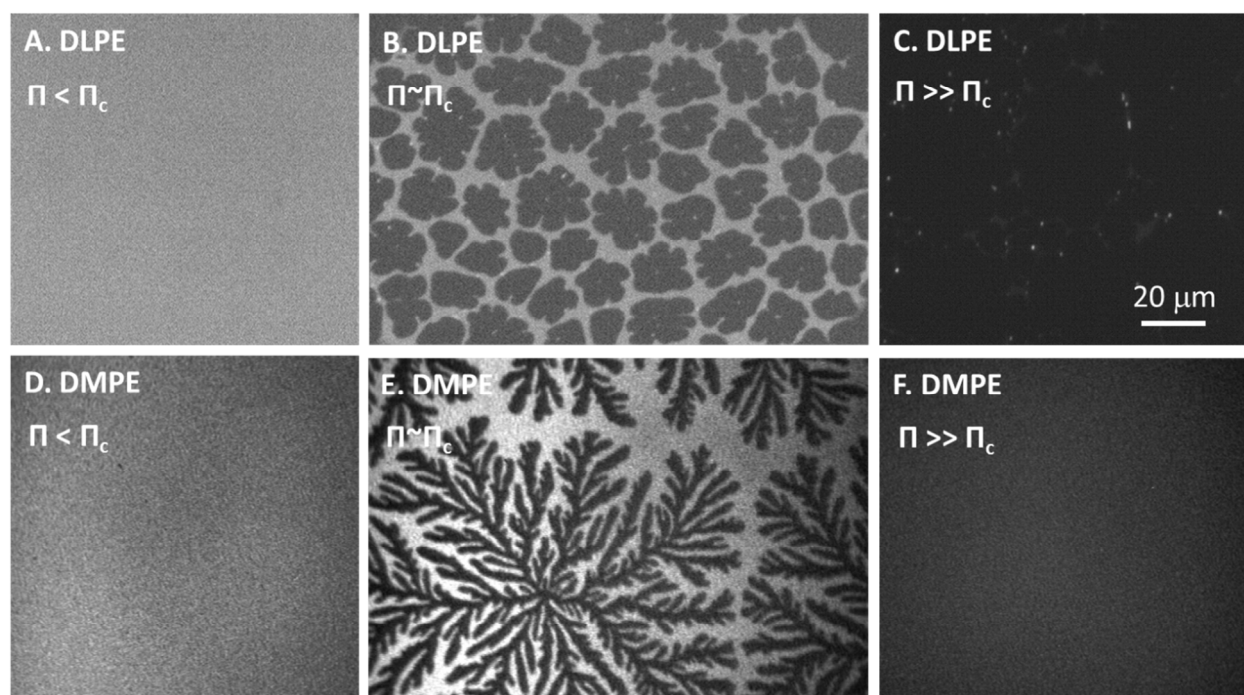

Figure2. The fluorescence micrographs of DLPE and DMPE at three different phases corresponding to the positions marked in the isotherm in Figure 1A. At $\Pi < \Pi_c$ (image A,D), the LE phase is uniformly fluorescent due to high solubility of the lipid dye in the disordered monolayer. At Π_c (image B, E) the LC phase nucleates as dark, multiple-armed structures (the better ordered LC phase excludes the lipid dye) in a bright, unstructured, continuous LE phase in which the lipid dye is concentrated. For $\Pi > \Pi_s$ (image C,F), both the LC and S phases are uniformly dark without distinguishable domains (the S phase also excludes the lipid dye); no changes in the images occur at Π_s.

GXID [34] shows that the tilt of the alkane chains of DMPE goes to zero at a surface pressure of ~ 35 mN/m, accompanied by a significant increase in the positional order (correlation length, ζ) from around 10 to 50-70 lattice spacings in DMPE films [5].

Figure 2 shows representative fluorescence microscopy images of the DLPE and DMPE monolayers; contrast in the images is due to the partitioning of 1 wt % Texas Red-DHPE into the disordered LE phase [42]. At surface pressures below Π_c, the LE phase is homogeneously bright, consistent with a uniform distribution of the fluorescent lipid in the disordered monolayer. The lack of any GIXD reflections in this phase is consistent with a lack of positional order [5]. As the surface pressure is increased, flower shaped or snowflake-shaped dark domains of LC phase start to nucleate, suggesting the presence of two-dimensional pseudo-hexagonal order. Contrast in these images is due to the greater solubility of the Texas Red-DHPE in the disordered LE phases compared to ordered LC phases [43-45]. With increasing compression or decreased mean molecular area in the LE-LC coexistence region, the LC domains grow in size but not in number at the expense of the LE phase; the snow-flaked shaped dark domains of DMPE grow via tip splitting until the tips start touching, at which point the domains grow in width. Compression in the LC region causes the dark LC domains to grow such that they are in contact with each other causing the appearance of uniformly dark films. No change in appearance occurs at Π_s; conventional fluorescence microscopy cannot detect this second-order phase transition between ordered phases.

Figure 3a (squares) presents the total friction factor, $f_r = f_w + f_s$, determined from the analysis of the characteristic time for rod rotation (Eqns. 3,4) as a function of surface pressure for a DLPE monolayer, along with the corresponding subphase friction factor, f_w (circles). This plot is a
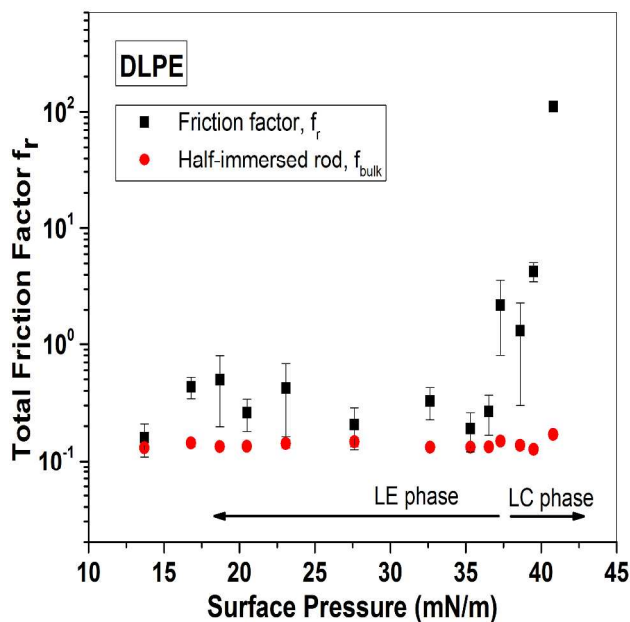
Figure 3a. The total friction factor, f_r and the friction factor due to the subphase water, f_w on a half-immersed rod at the air/lipid interface vs. surface pressure for DLPE samples. The total friction factor has been calculated using Eqn.3 in text. Below a surface pressure of $\Pi_c \sim 37$ mN/m, the monolayer is in the liquid expanded phase and has a low friction factor close to the f_w. Increasing the surface pressure above Π_c, the f_r is orders of magnitude higher than the f_w. In the LE region, $f_r \sim f_w$, indicating that there is no measureable viscosity change in this phase. The first order LE- LC transition is indicated by a sudden increase of f_r, indicating a corresponding reliable increase in the surface stresses. f_r values have been used to calculate the surface viscosity plotted in the Figure 3b, by using the theory of Fischer et al. for a infinitely thin cylinder at an interface.
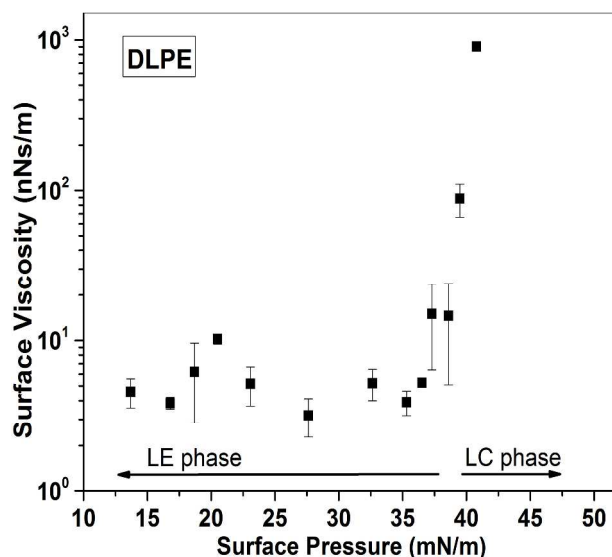

Figure 3b. Surface viscosity vs. surface pressure for a DLPE monolayer. Below a surface pressure of $\Pi_c \sim 37$ mN/m, the monolayer is in the liquid expanded phase and has a low viscosity consistent with the disordered molecular arrangements of the phase. Increasing the surface pressure above Π_c causes a sudden increase in the surface viscosity at the first order LE- LC transition. Each data point is an average of surface viscosity of multiple rods, and the error bars is the standard deviation of the data. The significant error bars at LE-LC coexistence indicate the heterogeneity of the surface in the LE-LC phase. Further increases in surface pressure cause the surface viscosity to increase exponentially. At surface pressures above 41mN/m, the monolayer acted like a solid; the rod stalled, and did not turn at all with increase in magnetic field.

15

representation of the decoupling of the contributions on the drag co-efficient from the bulk water

and the contributions from the surface drag. In turn, this decoupling of the contributions from the

bulk drag and the surface drag is the most accurate measure of the sensitivity of our instrument.

Figure 3a shows that for $\Pi < \Pi_c$, f_r is not significantly larger than f_w. Therefore it is not possible

to determine the absolute value of surface viscosity in this regime, except to say that $\eta_s \leq 5*10^{-9}$

N-s/m, the limit of sensitivity of the rheometer ($Bo \sim 1$, Eqn. 1). Figure 3b shows the calculated

values of surface viscosity as a function of surface pressure determined from f_s from Fig. 3a.

Within the experimental error, η_s does not change with increasing surface pressure in the LE

phase up to ~ 35 mN/m. However, there is an exponential increase in f_r for $\Pi > \Pi_c$, making f_r

$>> f_w$, and the drag on the probe is primarily due to η_s. Between 36 and 39 mN/m, η_s increased

by nearly two orders of magnitude, corresponding to the first order LE-LC phase transition. At

coexistence, the measured surface viscosity varied much more than in either the LE or LC phases

(large error bars in Fig. 3b). This is likely due to the location of the nanorod probes relative to

the coexisting LE or LC domains (Fig. 2); the location of the probes can lead to differences in

the local viscosity, as the rods are about the size of individual domains. In the LC phase, η_s

increases exponentially up to $\Pi \sim 41$ mN/m at which $\eta_s \sim 10^{-6}$ Ns/m. Increasing the surface

pressure further causes the rods to stop rotating entirely, consistent with an onset of surface

elasticity (Eqn. 6). However, the isotherm in Fig. 1 shows no evidence of an LC-S transition in
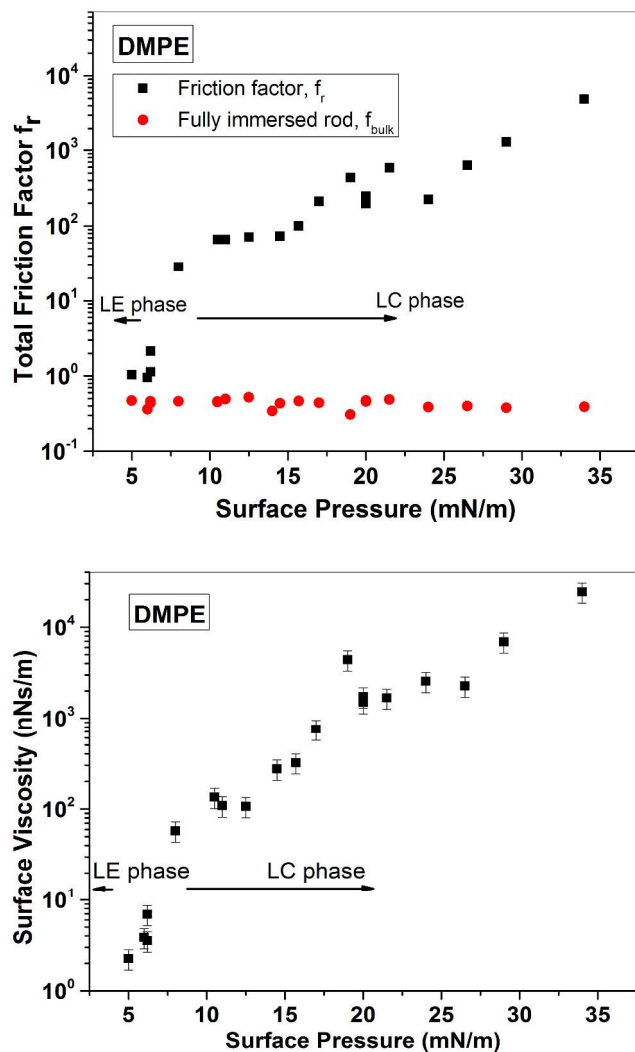
DLPE.

16

Figure 4a. The total friction factor, f_r and the friction factor due to the bulk water, f_w on a half-immersed rod at the air/lipid interface vs. surface pressure for DMPE films. The total friction factor has been calculated using Equ.3 in text. Below a surface pressure of $\Pi_c \sim 7$ mN/m, the monolayer is in the liquid expanded phase and has a low friction factor close to f_w. Increasing the surface pressure above Π_c, the f_r is orders of magnitude higher than the f_w. The first order LE- LC transition is indicated by a sudden increase of f_r and used to calculate the surface viscosity in Figure 4b.

Figure 4b. Surface viscosity vs. surface pressure for a DMPE monolayer. Below a surface pressure of 6-7 mN/m, the monolayer is in the liquid expanded phase and has a low viscosity consistent with the disordered molecular arrangements of the phase. Increasing the surface pressure above 7 mN/m causes an order of magnitude increase in the surface viscosity at the first order LE- liquid condensed (LC) transition. This discontinuous change in the surface viscosity can be correlated with a sharp dip in the surface compressibility modulus of the monolayer. Further increases in surface pressure cause the surface viscosity to increase exponentially. At a surface pressure of 32-34 mN/m, the transition to solid (S) phase occurs, although the surface viscosity still increases linearly, the phase transition is marked by the appearance of elasticity in the monolayer (See Fig. 5).

The LC phase is much more extensive in DMPE at room temperature, and the LC-S transition more obvious, making it more accessible to the rheometer (Fig. 4). As was the case for DPLE, Figure 4a shows that for $\Pi < \Pi_c$, $f_r \sim f_w$, while for $\Pi > \Pi_c$, $f_r > > f_w$. At $\Pi \sim \Pi_c$, there is an order of magnitude jump in f_r and η_s (Figure 4a and b between 7 and 8 mN/m), corresponding to the

17

LE-LC phase transition. For $\Pi > \Pi_c$, GIXD reveals distinct reflections indicating a two dimensional semi-crystalline ordering in the LC phase [5, 34]. Similar discontinuous changes in η_s were previously reported in fatty acid/alcohol monolayers at first order phase transitions from less ordered to more ordered phases [8, 9]. However, this discontinuity in the surface viscosity in a phospholipid monolayer has not been quantified before, as the surface viscosity at the LE-LC phase was beyond the sensitivity limit of macroscopic rheometers [18, 46, 47].
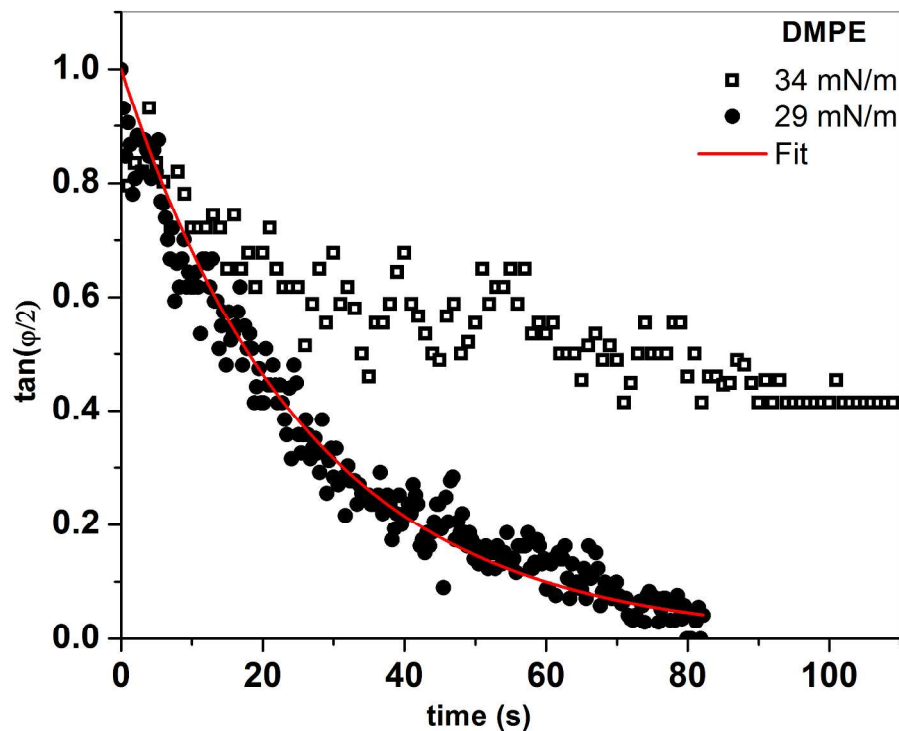

Figure 5. Rod reorientation at DMPE samples, tan ($\varphi/2$), vs. time, for surface pressures just below (circles, 29 mN/m) and above (squares, 34 mN/m) the LC-S phase transition at 32 mN/m (kink in isotherm, Fig. 1). At 29 mN/m, the nanorod reorients completely, ending at $\varphi = $ tan ($\varphi/2$) = 0, and the rate is consistent with a purely viscous response described by Eqn. 3. At 34 mN/m, above the LC-S transition surface pressure, the rod "stalls" at tan ($\varphi/2$) > 0, indicating the appearance of an elastic component, which causes the nanorod to stop rotating at a finite angle.

Between Π_c and Π_s, the surface viscosity increased exponentially with surface pressure, similar to DPPC, and mixed DPPC and cholesterol monolayers [39, 46, 48, 49]. However, even with the greatly increased surface viscosity, we were unable to detect any elasticity within the LC phase. The rod orientation decays exponentially with time (Eqn. 3) as expected for a purely viscous system (Fig. 5, circles), the rod aligns with the applied field at long times, and the decay curves overlap for perpendicular directions of applied torque (Supplemental Information). This overlap in the two decay curves also indicates that the rod motion did not damage structures in the film [39].

However, for $\Pi > \Pi_s \sim 34$ mN/m, the rod reorientation dynamics were not consistent with Eqn. 3 (Figure 5). The rod no longer reoriented parallel to the direction of the magnetic field, but stalled; tan ($\varphi/2$) did not decay to zero as would be expected from Eqn. 3 (circles). Further increases in surface pressure caused the rod to be completely immobile. These alterations in the rod response indicate an elastic contribution to the film in the S phase. GIXD of DMPE shows a transition from a tilted to untilted molecular orientation at Π_s [5, 34]. The translational order parameter increased gradually from ~ 10 lattice spacings at Π_c to $\sim$50-70 lattice spacings at Π_s [5]. Helm et al. suggest that the LC-S transition may be accompanied by a dehydration and ordering of the lipid head groups, in addition to the elimination of molecular tilt [5]. The abrupt appearance of elasticity in the monolayer shows that the LC-S transition is likely not just an elimination of tilt, but requires a significant change in the intermolecular interactions such as an ordering of the lipid head groups. Kim et al. reported that dipalmitoylphosphatidylcholine (DPPC) films at surface pressures between 12-14 mN/m also showed an onset of an exponential increase in elasticity that could correspond to a possible LC-S transition [38]. The slope of the surface viscosity vs. surface pressure also showed a change in slope at surface pressures between 12-14 mN/m,

19

consistent with a second order phase transition [38]. However, it is difficult to see any kink in DPPC isotherms, and DPPC molecules remain tilted at all surface pressures [50], which suggests that the LC-S transition likely involves the head group ordering rather than the tilt of the tail groups.
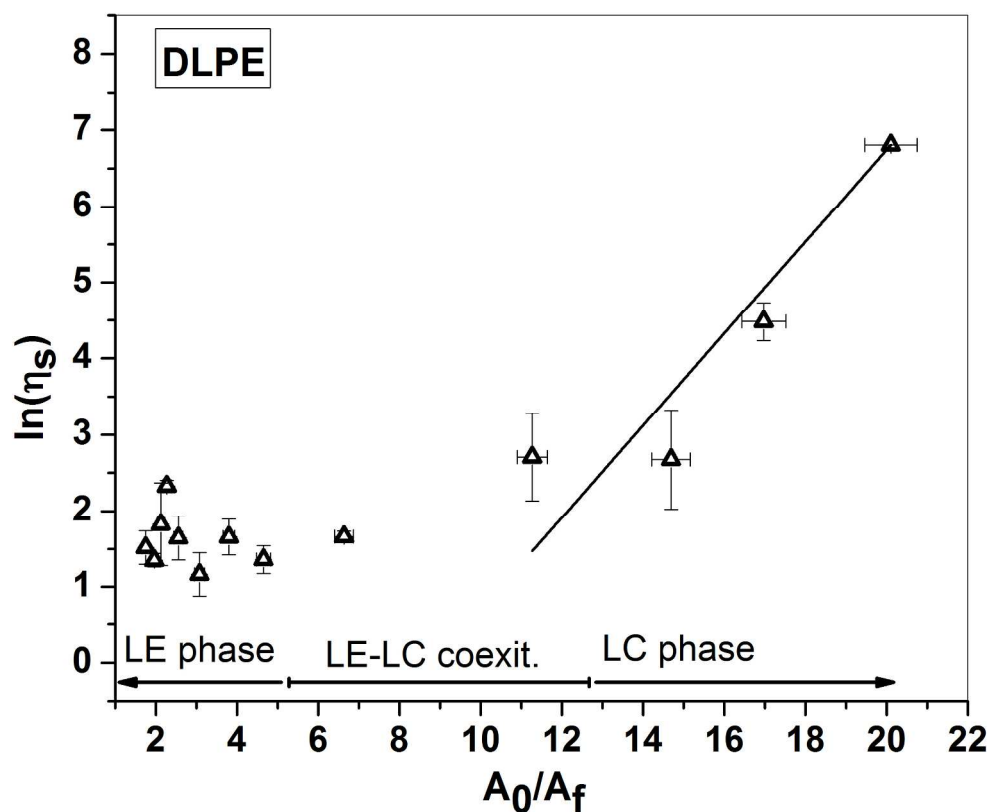

Figure 6a. Natural logarithm of surface viscosity vs. the ratio of the close-packed A_0 to free area A_f for DLPE monolayer. The correlation between surface viscosity and free-area model has been used to represent the phase transition. At $\Pi < \Pi_c$ the change in surface viscosity is not significant and does not satisfy the free area model. In the LC phase, the change in the surface viscosity with molecular area can be explained by the free area model ($p < 0.05$ for the fit).
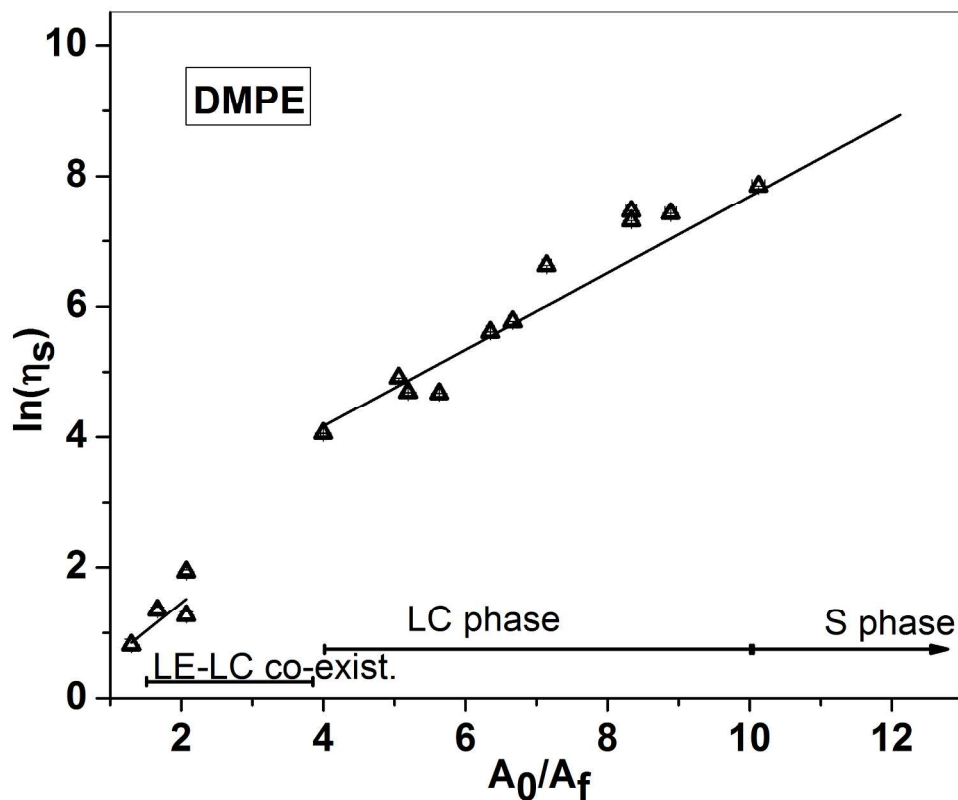
Figure 6b. Natural logarithm of surface viscosity vs. the ratio of the close-packed A_0 to free area A_f for DMPE monolayer. In the LC phase, the exponential increase in surface viscosity follows the two-dimensional free-area model ($p<0.1$).

The exponential increase in surface viscosity with surface pressure in the LC phase is consistent with the free area model previously used to correlate surface viscosity in DPPC[39, 49, 51, 52] and DPPC-cholesterol [53] films. Figure 6a-b represent a correlation of the surface viscosity with the free-area model [51]. The free area model is the two-dimensional analog of the classic free volume model developed to describe liquid viscosities [54] and is given by:

$$\ln \eta_s = \ln \eta_s^0 + \frac{BA_0}{A_f} \qquad (7)$$

The free area, A_f, is the difference between the measured area/molecule, A at a given Π, and the close-packed area/molecule, A_0: $A_f = A(\Pi) - A_0$. The parameter B in Eqn. 7 accounts for overlaps

of free volume in the original theory and ranges from $1/2 \leq B \leq 1$ [54]. We find that the value of B

makes little difference in the important fitting parameters of the model, so we set $B = \frac{1}{2}$ and used

A_0 and $\ln \eta_s^0$ as the two fitting parameters in Fig. 6. Table 1 shows that the values of the close-

packed molecular area, A_0, determined from the fits of the free area model to the surface

viscosity for both DLPE and DMPE LC phases correspond nearly exactly with the area/molecule

at the maximum compressibility (monolayer collapse) in Fig. 1b. This excellent agreement

between the area/molecule at the maximum compressibility and A_0 is consistent with the basic

assumptions used to derive the free area and free volume models [54]. The free area model also

correlates the limited surface viscosity data we have obtained in the LE phase of DMPE (Fig. 6).

Table 1: Fitting parameters from the free area model

	A_0(free area model) Å^2/molecule	A_0 (max. compressibility) Å^2/molecule	η_{s0} (nNs/m)
DLPE	43.6(1.4)	44.6	0.005
DMPE	40 (0.5)	40.6	6.11

Conclusions:

We present the detailed measured surface rheology of phosphatidylethanolamine monolayers

in the LE, LC and S phases, and the discontinuities in surface viscosity at the LE-LC first order

phase transitions. Over much of the disordered LE phases of DLPE and DMPE, the surface

viscosity is $< 10^{-9}$ Ns/m, which is below the sensitivity of the magnetic nanorod viscometer.

However, for both DLPE and DMPE, the surface viscosity undergoes a discontinuous jump at

the LE/LC phase transition, consistent with a first order phase transition and the onset of semi-

crystalline order in the LC phase (Fig. 2). Within the LC phase, the surface viscosity increases

exponentially with surface pressure (or decreasing area per molecule), with negligible surface elasticity. The surface viscosity in the LC phase of both DLPE and DMPE fit the free area model, with excellent agreement between the closed packed area/molecule predicted by the free area model and that given by the maximum in monolayer compressibility at monolayer collapse, even though the LC phase in DLPE only exists over a narrow range of surface pressure at room temperature.

A kink in the DMPE isotherm signifies an LC-S phase transition for $\Pi \sim$ 34-35 mN/m, and is accompanied by an abrupt onset of elasticity in the monolayer. GIXD shows that the molecular tilt in DMPE is eliminated at the LC-S transition, this transition between orthorhombic and hexagonal molecular packing may be the origin of the elasticity. The elimination of molecular tilt shows that the area occupied by the PE headgroup matches the area occupied by the crystalline alkane chains at the LC-S transition. We also observed an abrupt onset of surface elasticity in DLPE at ~40-41 mN/m, although no kink was observed in the DLPE isotherm. As DLPE and DMPE are chemically identical except for a two methyl group difference in chain length, we expect that DLPE also untilts at the LC-S transition as the areas occupied by the headgroup and crystalline alkane chains should be nearly identical to DMPE. However, we are not aware of any GIXD data on DLPE with which we can validate this hypothesis.

Interfacial microrheology is a sensitive tool to detect phase transitions and critical parameters in phospholipid films that are less obvious from isotherms. The correlation of elasticity with the elimination of molecular tilt in DMPE suggests that there is a previously unknown LC-S transition in DLPE. Interfacial rheology can be extremely useful in examining phase transition and molecular arrangements in monolayers that are difficult to examine by GIXD and its relative

23

simplicity allows for a much wider and more detailed examination of phospholipid monolayer structure.

References:

1. G. A. Jamieson and D. M. Robinson, *Mammalian Cell Membranes*, Butterworth, London, 1977.
2. R. F. Epand, P. B. Savage and R. M. Epand, *Biochemica et Biophysica Acta*, 2007, **1768**, 2500-2509.
3. O. Albrecht, H. Gruler and E. Sackmann, *J Phys-Paris*, 1978, **39**, 301-313.
4. V. M. Kaganer, H. Mohwald and P. Dutta, *Rev Mod Phys*, 1999, **71**, 779-819.
5. C. A. Helm, P. Tippmannkrayer, H. Mohwald, J. Alsnielsen and K. Kjaer, *Biophys. J.*, 1991, **60**, 1457-1476.
6. K. Kjaer, J. Alsnielsen, C. A. Helm, L. A. Laxhuber and H. Mohwald, *Phys. Rev. Lett.*, 1987, **58**, 2224-2227.
7. E. Boyd and W. D. Harkins, *J. Am. Chem. Soc.*, 1939, **61**, 1188-1195.
8. C. Alonso and J. A. Zasadzinski, *Journal of Physical Chemistry B*, 2006, **110**, 22185-22191.
9. G. T. Gavranovic, R. E. Kurtz, K. Golemanov, A. Lange and G. G. Fuller, *Ind. Eng. Chem. Res.*, 2006, **45**, 6880-6884.
10. R. E. Kurtz, M. F. Toney, J. A. Pople, B. H. Lin, M. Meron, J. Majewski, A. Lange and G. G. Fuller, *Langmuir*, 2008, **24**, 14005-14014.
11. K. S. Birdi, *Lipid and biopolymer monolayers at liquid interfaces.*, Plenum Press, New York, 1989.
12. P. G. Saffman and M. Delbruck, *Proc. Nat. Acad. Sci. USA*, 1975, **72**, 311-313.
13. V. Prasad, S. A. Koehler and E. R. Weeks, *Phys. Rev. Lett.*, 2006, **97**, 176001-176004.
14. S. Q. Choi, K. H. Kim, C. M. Fellows, K. D. Cao, B. Lin, K. Y. C. Lee, T. M. Squires and J. A. Zasadzinski, *Langmuir*, 2014, **30**, 8829-8838.
15. S. Y. Choi, S. Steltenkamp, A. J. Pascall, J. A. Zasadzinski and T. M. Squires, *Nature Communications*, 2011, **2**, 312.
16. K. Kim, S. Q. Choi, T. M. Squires and J. A. Zasadzinski, *Proc. Nat. Acad. Sci. USA*, 2013, **101**, E3054-E3061.
17. K. Kim, S. Q. Choi, J. A. Zasadzinski and T. M. Squires, *Soft Matter* 2011, **7**, 7782-7789.
18. J. Q. Ding, H. E. Warriner, J. A. Zasadzinski and D. K. Schwartz, *Langmuir*, 2002, **18**, 2800-2806.

19. C. F. Brooks, G. G. Fuller, C. W. Frank and C. R. Robertson, *Langmuir*, 1999, **15**, 2450-2459.
20. G. B. Bantchev and D. K. Schwartz, *Langmuir*, 2003, **19**, 2673-2682.
21. S. Reynaert, C. F. Brooks, P. Moldenaers, J. Vermant and G. G. Fuller, *J. Rheol.*, 2008, **52**, 261-285.
22. J. F. Klingler and H. M. McConnell, *J. Phys. Chem.*, 1993, **97**, 6096-6100.
23. D. K. Schwartz, C. M. Knobler and R. Bruinsma, *Phys. Rev. Lett.*, 1994, **73**, 2841-2844.
24. M. Sickert, F. Rondelez and H. A. Stone, *Epl*, 2007, **79**.
25. L. G. Wilson and W. C. K. Poon, *Phys Chem Chem Phys*, 2011, **13**, 10617-10630.
26. P. Dhar, Y. Y. Cao, T. M. Fischer and J. A. Zasadzinski, *Phys. Rev. Lett.*, 2010, **104**, -.
27. M. H. Lee, D. H. Reich, K. J. Stebe and R. L. Leheny, *Langmuir*, 2010, **26**, 2650-2658.
28. V. Prasad, S. A. Koehler and E. R. Weeks, *Phys Rev Lett*, 2006, **97**.
29. P. Dhar, T. M. Fischer, Y. Wang, T. E. Mallouk, W. F. Paxton and A. Sen, *Nano Letters*, 2006, **6**, 66-72.
30. R. Shlomovitz, A. A. Evans, T. Boatwright, M. Dennin and A. J. Levine, *Phys. Rev. Lett.*, 2013, **110**, 137802.
31. D. B. Allan, D. M. Firester, V. P. Allard, D. H. Reich, K. J. Stebe and R. L. Leheny, *Soft Matter*, 2014, **10**, 7051-7060.
32. T. M. Fischer, P. Dhar and P. Heinig, *J Fluid Mech*, 2006, **558**, 451-475.
33. C. A. Helm and H. Mohwald, *J. Phys. Chem.*, 1988, **92**, 1262-1266.
34. E. Maltseva and G. Brezesinski, *Chemphyschem*, 2004, **5**, 1185-1190.
35. W. F. Paxton, K. C. Kistler, C. C. Olmeda, A. Sen, S. S. K. Angelo, Y. Cao, T. E. Mallouk, P. E. Lammert and V. H. Crespi, *J. Am. Chem. Soc.*, 2004, **126**, 13424-13431.
36. P. Dhar, Y. Y. Cao, T. Kline, P. Pal, C. Swayne, T. M. Fischer, B. Miller, T. E. Mallouk, A. Sen and T. H. Johansen, *Journal of Physical Chemistry C*, 2007, **111**, 3607-3613.
37. P. Dhar, Y. Cao, T. M. Fischer and J. A. Zasadzinski, *Phys. Rev. Lett.*, 2010, **104**, 016001.
38. K. Kim, S. Q. Choi, J. A. Zasadzinski and T. M. Squires, *Soft Matter*, 2011, **7782-7789**, 7782-7789.
39. S. Q. Choi, S. Steltenkamp, J. A. Zasadzinski and T. M. Squires, *Nat Commun*, 2011, **2**, 312.
40. H. M. McConnell, *Annual Review of Physical Chemistry*, 1991, **42**, 171-195.
41. J. Israelachvili, *Langmuir*, 1994, **10**, 3774-3781.
42. M. Losche, E. Sackmann and H. Mohwald, *Ber. Bunsen-Ges. Phys. Chem. Chem. Phys.*, 1983, **87**, 848-852.
43. C. M. Knobler, *Science*, 1990, **249**, 870-874.
44. M. Losche and H. Mohwald, *Rev. Sci. Instrum.*, 1984, **55**, 1968-1972.
45. M. Losche, E. Sackmann and H. Mohwald, *Ber. Bunsen-Ges. Phys. Chem. Chem. Phys.*, 1983, **87**, 848-852.
46. E. Hermans and J. Vermant, *Soft Matter*, 2014, **10**, 175-186.
47. J. Kragel, G. Kretzschmar, J. B. Li, G. Loglio, R. Miller and H. Mohwald, *Thin Solid Films*, 1996, **284**, 361-364.
48. S. Q. Choi, K. Kim, C. M. Fellows, K. D. Cao, B. Lin, K. Y. Lee, T. M. Squires and J. A. Zasadzinski, *Langmuir*, 2014, **30**, 8829-8838.
49. K. Kim, S. Q. Choi, J. A. Zasadzinski and T. M. Squires, *Soft Matter*, 2011, **In press**.
50. K. Y. C. Lee, A. Gopal, A. von Nahmen, J. A. Zasadzinski, J. Majewski, G. S. Smith, P. B. Howes and K. Kjaer, *J Chem Phys*, 2002, **116**, 774-783.
51. C. Alonso and J. A. Zasadzinski, *Phys. Rev. E*, 2004, **69**, 0216021-0216026.
52. H. J. Galla, W. Hartmann, U. Theilen and E. Sackmann, *J Membr Biol*, 1979, **48**, 215-236.
53. K. Kim, S. Q. Choi, Z. A. Zell, T. M. Squires and J. A. Zasadzinski, *Proc Natl Acad Sci U S A*, 2013, **110**, E3054-3060.
54. M. H. Cohen and D. Turnbull, *J Chem Phys*, 1959, **31**, 1164-1169.

25